

Generating broadband second harmonics using TIR-QPM and guided wave optics approach – a comparative analysis with some important isotropic semiconductors

BHASWATI MEDHI, SUMITA DEB*

Department of Electrical Engineering, National Institute of Technology Agartala, Agartala-799046, Tripura, India

This paper is oriented towards a comparative study on three different isotropic semiconductor slab materials, viz., Gallium Arsenide (GaAs), Zinc Selenide (ZnSe) and Zinc Telluride (ZnTe), using the concept of highly multimodal nonlinear guided wave approach for understanding the second harmonic light generation (SHG) in the mid-infrared region (MIR) by total internal reflection quasi phase matching (TIR-QPM). The optical losses like the Goos-Hänchen (GH) shift, surface roughness and absorption loss along with the nonlinear law of reflection have been considered, when simulating the results in terms of peak conversion efficiency and 3dB bandwidth. The effect of nonlinear law of reflection is also incorporated when the slab is varied in terms of its length and thickness.

(Received July 18, 2017; accepted August 9, 2018)

Keywords: Guided wave optics, Second harmonic generation, Isotropic semiconductors, Non-linear law of reflection

1. Introduction

Quasi-phase-matching (QPM) is a technique commonly used for enhancing the efficiency of nonlinear frequency conversions, such as SHG, in those cases where perfectly phase matching condition cannot be achieved. The concept of TIR-QPM in a plane parallel slab was first introduced to the world by Armstrong et al. in 1992 [1], which has been later demonstrated in some isotropic semiconductors for resonant QPM – SHG by Boyd and Patel and Komine et al. and for non-resonant QPM towards Difference Frequency Generation (DFG) by Haidar et al. [2-4].

The main objective of this paper is to compare the characteristic features of the output performance when three different isotropic semiconductor materials are used under study to analyze the multimodal guided wave theory using TIR-QPM based broadband SHG in tapered slab configuration. The materials that we intend to compare are GaAs, ZnSe and ZnTe. The effect of the nonlinear reflection resulting in a complex destructive interference among the collinear and homogeneous second harmonics, as told by Raybaut et al [5], has also been incorporated in the analysis. Also they have mentioned in the same paper, the inadequacy of plane wave analysis to explain the nonlinear phenomenon where a spatial walk-off arises between the interacting waves which resulted into destructive interference when the waves moved back and forth in the slab interfaces and thus suggested to resort to guided wave analysis, where both the factors, namely, the non-collinearity and the GH shift between the interacting waves are taken into account. Along with these, the possibility of fine tuning of center wavelength of the SH spectra by varying the temperature, slab length and slab thickness for all the three materials have been explored. In

one of our published papers [6], this concept has been highlighted and hence the reported values of peak conversion efficiency and 3dB bandwidth are 0.024% and 103.2 nm respectively for a tapered structure of ZnTe crystal when the losses are considered. M. Raybaut et al in their paper [7] described that the homogeneous harmonic field is emitted at the interface by the nonlinear polarization vector in addition to the emission of the collinear harmonic field in order to satisfy the conservation of wave momentum parallel to the boundary. To fulfill our objective, a tapered isotropic semiconductor crystal slab has been chosen so that the successive bounce lengths will increase along the length of the slab, making a way for both resonant and non-resonant QPM.

2. Proposed scheme of analysis

A tapered geometry [8, 9] of the isotropic semiconductor slab has been used for SHG conversion using the phenomenon of TIR-QPM. In the tapered semiconductor slab, the base is taken parallel to the horizontal surface and the upper surface is tilted to an angle of θ . t_1 and t_2 are the vertical heights at the two end of the slab, t_1 being smaller than t_2 . When the fundamental optical beam is incident on the foremost slanted edge of the slab at an angle ψ , it gets refracted depending on the refractive index (RI) of the material and eventually strikes on the horizontal base surface of the slab. Total internal reflection of the optical radiation takes place within the slab when the respective angle of incidence ϕ_1 of the collimated beam is greater than the corresponding critical angle for the range of frequencies considered. The respective angle of incidence for both the fundamental and

the generated SH wave is determined depending on the wavelength dependent refractive index of the medium, RI being calculated by Sellmeier's Equation [10].

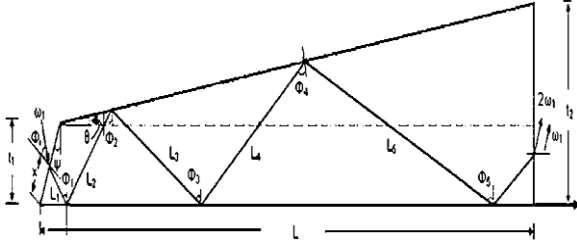


Fig. 1. Tapered isotropic semiconductor slab

The analysis has been carried out considering 'p-p-p' as the polarization direction for the two fundamental beam as well as the generated SH beam. In p-p-p polarization configuration, the net phase shift tends to approach the numerical value of π in a very rapid way over a wide range of incidence angle. In this present analysis, as the angle of incidence varies, at each bounce of TIR, so the effective non-linear co-efficient also varies at each reflection. Also, the effective d- coefficient for ppp polarized radiation for the angle τ at the plane of incidence with the slab orientation in the [001] direction is given by

$$d_{ppp} = 6d_{ij} \cos^2 \phi_n \sin \phi_n \cos \tau \sin \tau \quad (1)$$

Now, in this paper we have chosen three different isotropic semiconductors, namely, GaAs, ZnSe and ZnTe, all falling under $\bar{4}3m$ symmetry class, therefore the value of d_{ij} would correspond to d_{14} value of the respective materials. The various optical properties of the mentioned materials are shown in Table 1.

3. Application of multimodal guided wave approach

It has been observed that various physical phenomenon brought out the adequacy of a plane wave analysis for Fresnel Phase Matching. Many of the earlier works are done using the plane wave optics [9-13] using the tapered geometry of the slab, but the merit lies in using the guided wave analysis as it takes both the factors – (i)

the non-collinearity of the waves, and (ii) the Goos-Hänchen shift into account in a built-in way thus, giving more accurate results as said by Raybaut et al. The slab which once acted as the bulk structure would now act as the guide as soon as many hundreds of modes are envisaged into it.

In order to focus on main physical insights, ppp-polarization of the beams has been chosen. Here, the polarization vectors are oriented in the xz-plane and the waves are travelling in the z-direction. The pump and the output field distributions are given by:

$$\begin{aligned} E_y^\omega(x, z, t) &= \sum_l A_l^\omega(z) E_l^\omega(x) e^{-i(\omega t - \beta_l^\omega z)} e_y + cc \\ E_y^{2\omega}(x, z, t) &= \sum_m A_m^{2\omega}(z) E_m^{2\omega}(x) e^{-i(2\omega t - \beta_m^{2\omega} z)} e_y + cc \end{aligned} \quad (2)$$

Where, A_l^ω - varying amplitude of mode l in the input field,

$A_m^{2\omega}$ - varying amplitude of mode m in the output field,

E_l^ω - lth order TM wave function of the input field,

$E_m^{2\omega}$ - mth order TM wave function of the output field,

β_l^ω - propagation constant for the input field

$$(\beta_l^\omega = \sqrt{(n_\omega k_\omega)^2 - (l \frac{\pi}{t})^2},$$

$\beta_m^{2\omega}$ - propagation constant for the output field

$$(\beta_m^{2\omega} = \sqrt{(2n_{2\omega} k_\omega)^2 - (m \frac{\pi}{t})^2})$$

Assuming 't' as the waveguide thickness, the transverse and the evanescent wavenumbers, are given by $\alpha_l^\omega = \sqrt{(n_\omega k_\omega)^2 - (\beta_l^\omega)^2}$ and $k_l^\omega = \sqrt{(\beta_l^\omega)^2 - (k_\omega)^2}$ respectively. For maximum $A_0^l(0)$, the incidence angle has to be set at $l \approx l_\theta$, meaning that only 10-20 modes can participate amongst the large number of modes propagated through the guide. Now, when $A_l^\omega(z) = A_l^\omega(0) = A_l^\omega$ for an un-depleted pump approximation, the coupling mode equations can be derived as shown by Yariv [14]. The output field equation of the generated SH can be represented as:

Table 1. Optical properties of the isotropic materials chosen for comparative study

Semiconductor materials	Crystal symmetry class	d- coefficient (pm/V)	Absorption coefficient (cm ⁻¹)	p-v value (nm)	Transparency range (μm)
GaAs	$\bar{4}3m$	107 [16, 17]	0.02 [20]	4 [23]	1-15 [16]
ZnSe	$\bar{4}3m$	25 [18]	5×10^{-4} [21]	150 [24]	0.5-14 [18]
ZnTe	$\bar{4}3m$	90 [19]	0.008 [22]	30 [25]	0.6-25 [22]

$$A_{m,x}^{2\omega}(x) = \frac{-\omega\epsilon_0}{p_0} \chi_{yyy}^{(2)} \sum_{l'} \sum_l S_{l,l',m} (A_{l,y}^\omega, A_{l',y}^\omega) L \frac{\exp(i\delta\beta_{l,l',m} L) - 1}{\delta\beta_{l,l',m} L} \quad (3)$$

where p_0 is the normalizing power constant which corresponds to 1 W/m in the y -direction. $\chi_{yyy}^{(2)}$ is the nonlinear susceptibility tensor, which must not be zero. The overlap integral ($S_{l,l',m}$) plays an important role in keeping the parity of the interacting waves, therefore $S_{l,l',m}$ between the modes must be optimized. It can be written as:

$$S_{l,l',m} = (-1)^m \frac{(-1)^{l+l'-(m+1)}}{l+l'-m} \frac{8}{2\pi} \sqrt{\frac{2}{t\beta_{l,x}^\omega \beta_{l',x}^\omega \beta_{m,x}^\omega}} (\omega\mu_0 p_0)^{\frac{3}{2}} \quad (4)$$

It is much enhanced for very small values of Δ ($|\Delta|=1$) where $\Delta = l+l'-m$ is the mode mismatch and it is an odd integer. But if Δ takes larger values, it tends to correspond to lower spatial overlap between the interacting waves.

The phase mismatch ($\beta_{l,l',m}$) is another important factor which can be derived from Synder-De la Rue approximation:

$$\beta_{l,l',m} = \frac{n_\omega k_\omega \cos\theta}{t\beta_{l,x}^\omega} \left[\frac{2n_\omega \cos\theta_l}{\sqrt{(n_\omega^2-1)}} \left(\frac{1}{K_l} + \frac{1}{K_{l'}} - \frac{1}{K_m} \right) - \Delta\pi - \frac{t/\cos\theta_l}{\Lambda_c} \pi \right] \quad (5)$$

where K_l - describes Fresnel birefringence, which corresponds to 1 if TE polarization or n_ω^2 if TM polarization and Λ_c - coherence length in SHG, given by

$$\Lambda_c = \frac{\lambda}{4(n_{2\omega} - n_\omega)}.$$

The mode amplitude which is denoted by A_ω^l is given by:

$$A_\omega^l = 2iL \sqrt{\frac{\omega\mu_0}{\beta_{l,t}} p_0} \frac{\sqrt{\pi}}{2\omega} \sin\theta e^{-F(l)^2} \left[\text{Erfi} \left\{ F(l) - i \frac{\sin\theta}{2} \frac{t}{\omega_0} \right\} - \text{Erfi} \left\{ F(l) + i \frac{\sin\theta}{2} \frac{t}{\omega_0} \right\} \right] \quad (6)$$

Where ω_0 is the beam waist of the incident Gaussian beam and $F(l)$ is a function which is represented by

$$F(l) = \frac{1}{2} \frac{\omega_0}{\sin\theta} (k_\omega \cos\theta - l \frac{\pi}{t}) \quad \text{and} \quad \text{Erfi}(z) = -i\text{Erfi}(iz),$$

$\text{Erf}(z)$ being the error function. The wave-guiding condition for an infinitely confining wave is $F(l) \approx 0$ where the mode amplitude is maximal. Moreover, the number of excited modes is roughly given by $\Delta t = \frac{4t \sin\theta}{\pi\omega_0}$

, implying that only a few (approximately 10) number of modes is actually involved in the phenomenon [5].

4. Analysis in the perspective of Nonlinear Law of Reflection

M. Raybaut has pointed out the Law of Nonlinear Reflection in his paper [15] which was noted by Bloembergen and Pershan as the basic reason for the drop in conversion gain of the parametric oscillations in a plane parallel plate. According to this law, when a beam of light is incident on any nonlinear medium, a non-collinear propagation of the fundamental and the generated SH wave takes place where some walk-off is introduced between the waves, which results in destructive interference patterns while moving back and forth between the interfaces. This law of nonlinear reflection emerges from the phenomenon that a homogeneous harmonic field is emitted at the interface by the nonlinear polarization vector in addition to the emission of the collinear harmonic field in order to satisfy the conservation of wave momentum parallel to the boundary. This law satisfies the Snell- Descartes law which is expressed for a SHG is:

$$n_\omega \sin(\phi_\omega) = n_{2\omega} \sin(\phi_{2\omega}) \quad (7)$$

Where, n_ω and $n_{2\omega}$ are the refractive indices at the fundamental and generated SH respectively, ϕ_ω and $\phi_{2\omega}$ are the respective angles of incidence of the fundamental and SH beam at the interface.

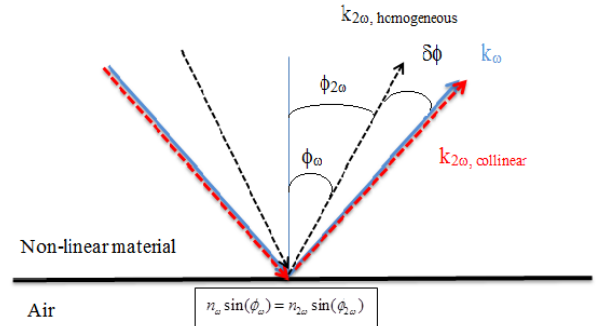


Fig. 2. Emission of collinear and homogeneous SH waves at air-nonlinear material interface according to the law of TIR

The small variation in incidence angle $\delta\phi$ by a first order expansion is given by $\delta\phi = -(\frac{\delta n}{n}) \tan\phi_\omega$, where $\delta n = n_{2\omega} - n_\omega$ is the optical dispersion and $n \approx n_{2\omega} \approx n_\omega$.

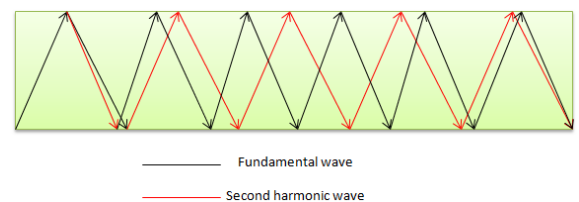


Fig. 3. Recombination of the pump and SH beam in plane parallel slab

As demonstrated by Raybaut et al [5], the nonlinear waves traverse in a non-collinear way due to the reciprocal lattice vector due to periodic Fresnel phase shift at the interfaces throughout the parallel slab (Fig. 3). Since there is a certain separation in angle between the pump and SH field, which depends on the optical dispersion and the respective angle of incidence, there is a spatial walk-off that reduces the overlap between the interacting waves. Moreover, after propagating for a definite number of bounces, the fundamental and the generated SH waves may recombine, expressed by Eq. (8), leading to a complex destructive interference like situation which again is the reason behind low conversion yield.

$$N_{rec} \approx 2 \left| \frac{\tan \phi_\omega}{\delta \phi} \right| \approx 2 \left| \frac{n}{\delta n} \right| \quad (8)$$

5. Results and discussion

A computer aided simulation has been carried out using MATLAB platform for the nonlinear multimodal analysis in a tapered rectangular structured waveguide for three different isotropic semiconductors – GaAs, ZnTe and ZnSe considering the input fundamental broadband source of 6-10.6 μm with a fundamental beam intensity of 10 MW/cm². The semiconductor slab parameters that has been considered for the analysis are as follows – the slanted slab angle with respect to the horizontal base $\psi = 0.4^\circ$, length of the slab $L=10$ mm, the shorter vertical height is kept constant at $t_1 = 400$ μm and the taller height t_2 is variable with respect to the tapering angle θ . The temperature is maintained at 300 K for the entire process. Moreover, the analysis is made using the concept of multimodal nonlinear guided wave theory in lieu of plain ray optics. The comparative analysis presented in this paper is based on two analyses – at first, the SH conversion efficiency (in %) and 3dB bandwidth (in nm) has been studied for an absolute ideal condition for the mentioned three semiconductor materials. Secondly, the same configuration of the slab has been analyzed with the same three semiconductor materials considering the losses of surface roughness, GH shift and absorption in the light of nonlinear law of reflection. In the latter case, a significant drop in peak efficiency is observed (Figs. 4, 5, 6 and Table 2) as compared to the ideal one.

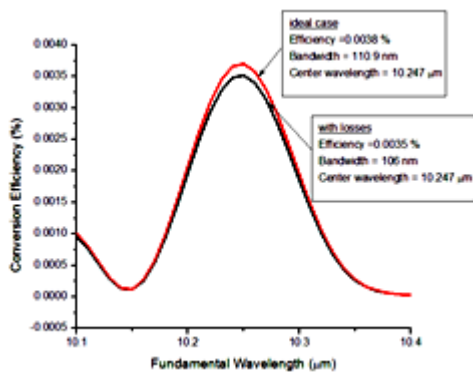


Fig. 4. Graphical representation of broadband SHG in GaAs isotropic semiconductor in a tapered waveguide

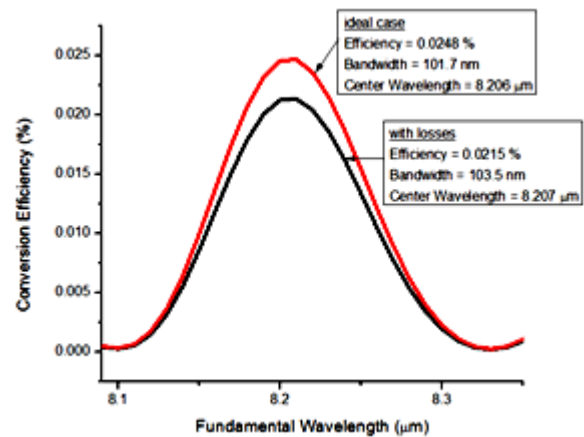


Fig. 5. Graphical representation of broadband SHG in ZnTe isotropic semiconductor in a tapered waveguide

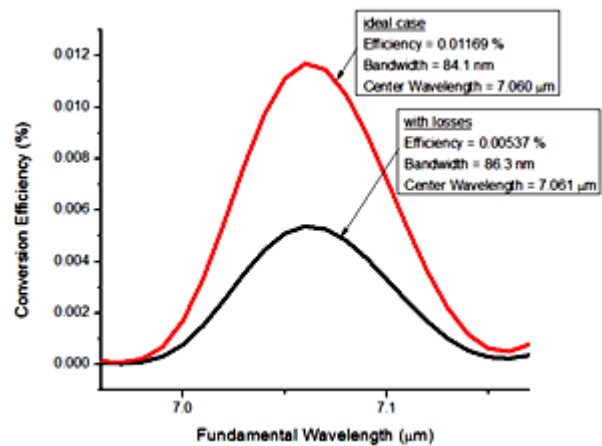


Fig. 6. Graphical representation of broadband SHG in ZnSe isotropic semiconductor in a tapered waveguide

5.1. Effect of variation in slab thickness

To check the effect on the functioning parameters of the tapered configuration when the slab thickness is changed, we have kept the lower vertical height t_1 fixed and then changed the inclination angle ϕ values so that the higher vertical height t_2 can take admissible values which in turn will change the slab thickness. As the slab thickness is increased, we have found that the efficiency for GaAs, ZnTe and ZnSe does not follow a definite pattern, it increases and decreases at intervals but the bandwidth in GaAs and ZnSe semiconductors is found to be dropping gradually with increase in slab thickness. Again for, ZnTe semiconductor, just like the efficiency, the bandwidth too does not follow any definite pattern. This is because of the effect of nonlinear law of reflection, as mentioned earlier in the section 4, where both constructive and destructive interference holds good in the conversion process, depending on the total interaction length. Figs. 7, 8, 9 and Table 3 shows the data.

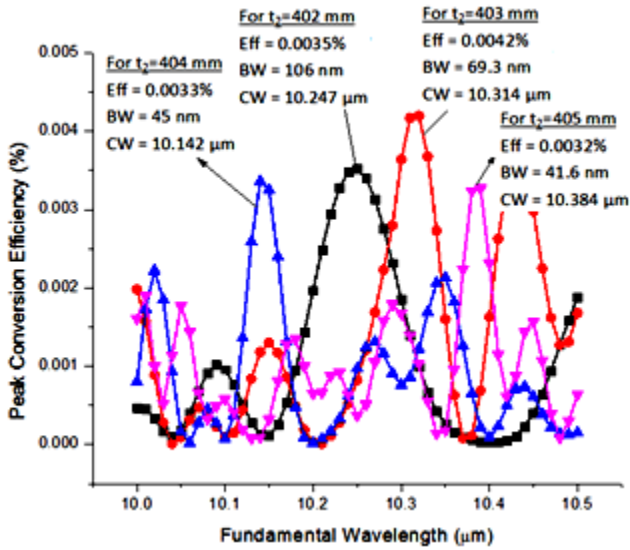


Fig. 7. Graphical representation of GaAs semiconductor tapered slab when the slab thickness is varied and nonlinear law of reflection and optical losses are included

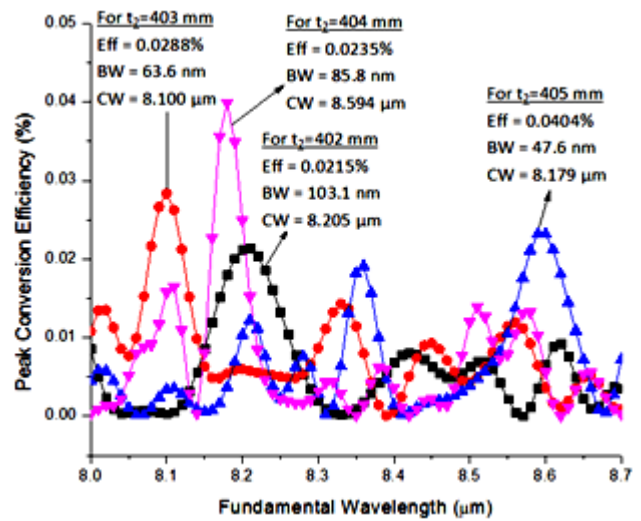


Fig. 8. Graphical representation of ZnTe semiconductor tapered slab when the slab thickness is varied and nonlinear law of reflection and optical losses are included

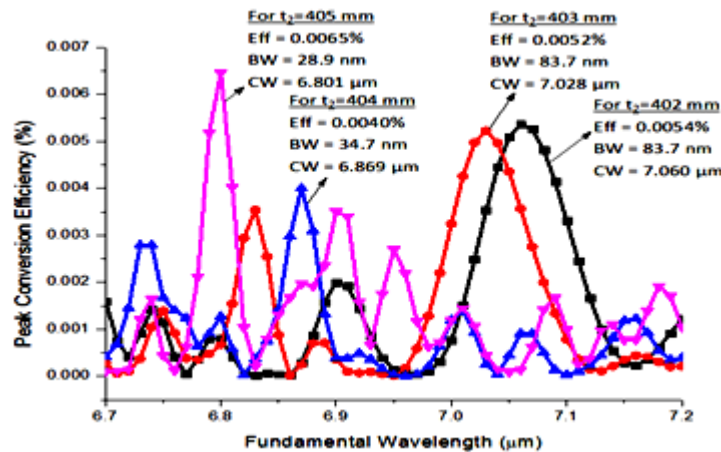


Fig. 9. Graphical representation of ZnSe semiconductor tapered slab when the slab thickness is varied and nonlinear law of reflection and optical losses are included

Table 2. Comparative analysis of broadband SHG of GaAs, ZnTe and ZnSe waveguide when losses inclusive of nonlinear law of reflection are considered with that of ideal case

Semiconductor material	Without any loss			With optical losses including nonlinear law of reflection		
	Peak Conversion Efficiency (%)	3dB Bandwidth (nm)	Center wavelength of fundamental (μm)	Peak Conversion Efficiency (%)	3dB Bandwidth (nm)	Center wavelength of fundamental (μm)
GaAs	0.0038	110.9	10.247	0.0035	106.0	10.247
ZnTe	0.0248	101.7	8.206	0.0215	103.5	8.207
ZnSe	0.0116	84.1	7.060	0.0053	86.3	7.061

Table 3. Comparative analysis of broadband SHG of GaAs, ZnTe and ZnSe waveguide when the slab thickness is varied and nonlinear law of reflection and optical losses are included

t ₁ (μm)	t ₂ (μm)	(t ₂ -t ₁) (μm)	Peak Conversion Efficiency (%)			3dB Bandwidth (nm)			Center wavelength of fundamental (μm)		
			GaAs	ZnTe	ZnSe	GaAs	ZnTe	ZnSe	GaAs	ZnTe	ZnSe
400	402	2	0.0035	0.0215	0.0054	106	103.5	83.7	10.247	8.205	7.060
400	403	3	0.0042	0.0288	0.0052	69.3	63.6	83.7	10.314	8.100	7.028
400	404	4	0.0033	0.0235	0.0040	45	85.8	34.7	10.142	8.594	6.869
400	405	5	0.0032	0.0404	0.0065	41.6	47.6	28.9	10.384	8.179	6.801

5.2. Effect of variation in slab length L

As discussed in the earlier sections, the conversion efficiency depends on the length between the consecutive TIR bounces throughout the slab. For our tapered slab configuration, the value of $\frac{\delta n}{n}$ will remain fixed but the angle of incidence $\delta\phi$ will go on increasing at each bounce point, thereby increasing the separation between the homogenous and the collinear SH beams, which denotes destructive interference taking place. But since, recombination occurs after the waves travel a certain slab length due to the effect of nonlinear law of reflection, therefore constructive interference also comes into the picture. For this reason, the SH conversion efficiency and bandwidth does not follow an even pattern. With the increase in slab length, the efficiency as well as the bandwidth has been seen to be increasing and dropping due the simultaneous effect of constructive and destructive interferences. Fig. 10, 11, 12 and Table 4 depicts the results of variation in slab length.

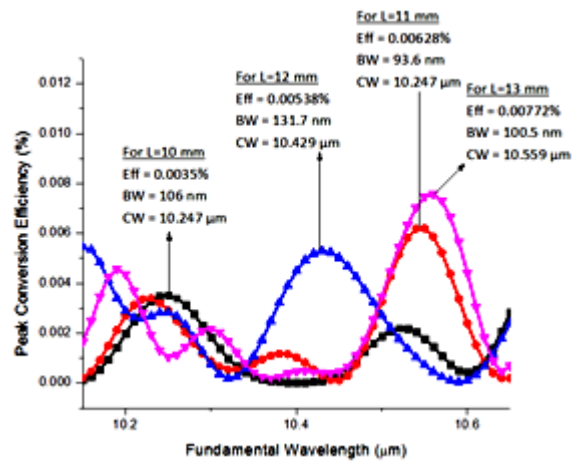


Fig. 10. Graphical representation of GaAs semiconductor tapered slab when the slab length is varied incorporating losses

Table 4. Comparative analysis of broadband SHG of GaAs, ZnTe and ZnSe waveguide when the slab length is varied and nonlinear law of reflection and optical losses are included

t ₁ (μm)	t ₂ (μm)	Slab length L (mm)	Peak Conversion Efficiency (%)			3dB Bandwidth (nm)			Center wavelength of fundamental (μm)		
			GaAs	ZnTe	ZnSe	GaAs	ZnTe	ZnSe	GaAs	ZnTe	ZnSe
400	402	10	0.0035	0.0215	0.0054	106	103.5	83.70	10.247	8.205	7.060
		11	0.0062	0.0283	0.0021	93.6	107.5	72.74	10.544	7.964	7.077
		12	0.0053	0.0351	0.0018	131.7	79.72	83.18	10.429	8.136	7.093
		13	0.0077	0.0176	0.0016	100.5	65.85	63.90	10.559	8.136	7.385

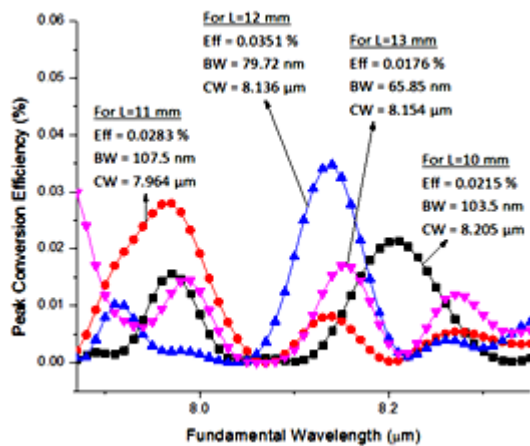


Fig. 11. Graphical representation of ZnTe semiconductor tapered slab when the slab length is varied and nonlinear law of reflection and optical losses are included

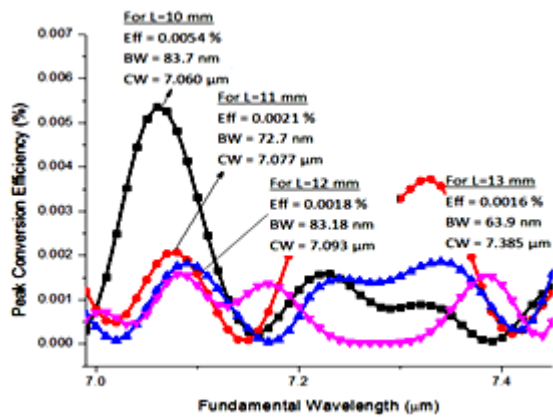


Fig. 12. Graphical representation of ZnSe semiconductor tapered slab when the slab length is varied and nonlinear law of reflection and optical losses are included

6. Conclusion

This paper reports a comparative study with three of the $\bar{4}3m$ categorized isotropic semiconductors (GaAs, ZnTe and ZnSe) on a tapered slab configuration using the concept of multimodal guided wave theory where the effects on SH efficiency and 3dB bandwidth are analyzed in ideal condition and in condition where optical losses like surface roughness, GH shift and absorption are considered including the law of nonlinear reflection in the conversion process. The destructive interference due to the nonlinear law of reflection is well described in this paper. When the law of nonlinear reflection is considered, there is always a recombination of the parametric beams resulting in destructive interference pattern along with the constructive one. Destructive interference effect is quite dominant as spatial walk-off is more prominent in this type of structure. Also, it has been observed that because of this law there is a significant decrease in the peak

conversion efficiencies in all the three materials. Again, the effects are demonstrated here when the slab thickness and the length of the slab is varied. ZnTe seems to fair out of the three materials chosen in terms of efficiency, though with proper choice of the related operating conditions, one can design an efficient broadband frequency converter of desired bandwidth in various spectral regions particularly in mid-IR region depending on the applications in the field of IR thermography, IR spectroscopy, coherent control, imaging, etc.

References

- [1] J. A. Armstrong, N. Bloembergen, J. Ducuing, P.S. Pershan, Phys. Rev. **127**, 1918 (1962).
- [2] G. D. Boyd, C. K. N. Patel, Appl. Phys. Lett. **8**, 313 (1966).
- [3] H. Komine, W. H. Long Jr., J. W. Tully, E. A. Stappaerts, Opt. Lett. **23**, 661 (1998).
- [4] R. Haidar, N. Forget, P. Kupecek, E. Rosencher, J. Opt. Soc. Am. B **21**, 1522 (2004).
- [5] M. Raybaut, A. Godard, A. Toulouse, C. Lubin, E. Rosencher, Opt. Express **16**, 18457 (2008).
- [6] B. Medhi, S. Deb, Optik **135**, 426 (2017).
- [7] M. Raybaut, A. Godard, R. Haidar, M. Lefebvre, Ph. Kupecek, Ph. Lemasson, E. Rosencher, Appl. Phys. Lett. **92**, 121112-1 (2006).
- [8] A. Saha, S. Deb, Opt. Comm. **284**, 4714 (2011).
- [9] S. Deb, A. Saha, Optik **126**, 3371 (2015).
- [10] H. H. Li, J. Phys. Chem. Ref. Data **13**, 103 (1984).
- [11] M. Deb Barma, S. Deb, A. Saha, J. Nonlinear Opt. Phys. & Mater. **24**, 1550041-1 (2015).
- [12] S. Banik, S. Deb, A. Saha, Opt. Comm. **287**, 196 (2013).
- [13] S. Banik, U. Das, S. Deb, A. Saha, Opt. Comm. **295**, 180 (2013).
- [14] A. Yariv, IEEE J. Quant. Electron. **QE-9**, 919 (1973).
- [15] N. Bloembergen, P. S. Pershan, Phys. Rev. **128**, 606 (1962).
- [16] T. Skauli, P. S. Kuo, K. L. Vodopyanov, T. J. Pinguet, O. Levi, L. A. Eyres, J. S. Harris, M. M. Fejer, J. Appl. Phys. **94**, 6447 (2003).
- [17] T. Skauli, K. L. Vodopyanov, T. J. Pinguet, A. Schober, O. Levi, L. A. Eyres., M. M. Fejer, J. S. Harris, B. Gerard, L. Becouarn, E. Lallier, G. Arisholm, Opt. Lett. **27**, 628 (2002).
- [18] A. Mustelier, E. Rosencher, Ph. Kupecek, A. Godard, M. Baudrier, M. Lefebvre, M. Poulat, G. Mennerat, C. Pasquer, Ph. Lemasson, Appl. Phys. Lett. **84**, 4424 (2004).
- [19] R. L. Sutherland, "Handbook of nonlinear optics", Marcel Dekker, New York, 1975.
- [20] <http://www.almazoptics.com/GaAs.htm>, May 2016.
- [21] B. Imangholi, M. P. Hasselbeck, M. Sheik-Bahae, Opt. Comm. **227**, 337 (2003).
- [22] <http://www.ClevelandCrystals.Inc.II-VICrystals.htm>, May 2016.
- [23] R. Haidar, Ph. Kupecek, E. Rosencher, Appl. Phys. Lett. **83**, 1506 (2003).
- [24] R. Haidar, Ph. Kupecek, E. Rosencher, R. Triboulet, Ph. Lemasson, Opto-electron. Rev. **11**, 155 (2003).
- [25] N. Lovergine, D. Manno, A. M. Mancini, L. Vasaneli, J. Cryst. Growth **128**, 633 (1993).

*Corresponding author: bhaswatimtech@gmail.com, sumita_nita@rediffmail.com